



# **Novel Graphitic Carbon Nitride/Co-B-P Nanocomposites with Significantly Enhance Visible-Light Photocatalytic Hydrogen Production from Water Splitting**

**Miza A. Kombo <sup>a\*</sup>, Abdul A.J Mohamed <sup>a</sup>,  
Suleiman A. Suleiman <sup>b</sup> and An-Wu Xu <sup>c</sup>**

<sup>a</sup> *Department of Natural Science, School of Natural and Social Sciences, The State University of Zanzibar, P.O.Box 146, Zanzibar, Tanzania.*

<sup>b</sup> *Tanzania Atomic Energy Commission, Directorate of Radiation Control, P.O. Box 743, Arusha, Tanzania.*

<sup>c</sup> *Department of Chemistry Physics, Division of Nanomaterials and Chemistry, Hefei National Laboratory for Physical Sciences at the Microscale, University of Science and Technology of China, Hefei, 230026, People's Republic of China.*

## **Authors' contributions**

*This work was carried out in collaboration among all authors. All authors read and approved the final manuscript.*

## **Article Information**

DOI: 10.9734/CSJI/2024/v33i3895

## **Open Peer Review History:**

This journal follows the Advanced Open Peer Review policy. Identity of the Reviewers, Editor(s) and additional Reviewers, peer review comments, different versions of the manuscript, comments of the editors, etc are available here: <https://www.sdiarticle5.com/review-history/115156>

**Original Research Article**

**Received: 07/02/2024**

**Accepted: 12/04/2024**

**Published: 30/04/2024**

## **ABSTRACT**

As a promising metal-free photocatalyst for hydrogen (H<sub>2</sub>) production through water splitting under visible-light irradiation, graphitic carbon nitride (g-C<sub>3</sub>N<sub>4</sub>) photocatalysts decorated with CoBP was prepared via simple ultra sonification. This paper highlights the structures of the photocatalysts,

\*Corresponding author: E-mail: mizakombo@yahoo.com;

their stability, rate of hydrogen evolution and the mechanism of charge transfer within the photocatalysts. The prepared  $C_3N_4/CoBP$  nanocomposite photocatalysts were characterized by using X-ray diffraction, X-ray photoelectron spectroscopy, transmission electron microscopy, scanning electron microscopy and UV–visible (UV–vis) diffuse reflectance spectroscopy. After detailed analysis, the  $C_3N_4/CoBP$  nanocomposite photocatalysts showed excellent photocatalytic performance, which was due to the formation of the heterostructured hybrids of g- $C_3N_4$  and CoBP. The effects of  $C_3N_4/CoBP$  nanohybrids on  $H_2$  evolution were evaluated. The effects improved with increasing load of CoBP until the optimal level (5 wt% CoBP with visible-light irradiation at  $\lambda \geq 420$  nm). The maximum and remarkable photocatalytic  $H_2$  evolution rate of  $51.68 \mu\text{mol h}^{-1}$  was achieved, which was 3.8 times that obtained from pure g- $C_3N_4$ . Moreover, the  $C_3N_4/CoBP$  heterostructured nanohybrids demonstrated extremely high photostability and recyclability for  $H_2$  evolution after visible light illumination. The composite hybrid accelerated the separation and transfer of photogenerated charge carriers and subsequently suppressed charge recombination. Conclusively, this study offered an opportunity for the design and synthesis of highly stable and efficient  $C_3N_4/CoBP$  nanocomposite photocatalysts for energy conversion and utilisation.

**Keywords:** *Heterostructured photocatalyst;  $C_3N_4/CoBP$  nanocomposite; water splitting; hydrogen evolution; charge separation efficiency.*

## 1. INTRODUCTION

“Hydrogen ( $H_2$ ) is considered as a clean, renewable, environmental friendly and attractive alternative energy source compared with fossil fuels” [1,2]. “After Fujishima and Honda reported photoelectrochemical water splitting over a  $TiO_2$  electrode in 1972, photocatalytic  $H_2$  production via water splitting under solar irradiation has become the most fascinating and promising strategies for solving the energy crisis and environmental pollution” [3–6]. In the past few years, extensive effort has been devoted to designing and developing various semiconductor-based photocatalysts for  $H_2$  production via water splitting. It includes but not limited to oxides [7], sulphides [8], nitrides [2] and conjugated polymer [9,10]. “However, most of these materials are limited for practical requirements because of low efficiency, poor chemical stability and high costs” [4,5,9]. Therefore, to improve the efficiency of photocatalytic  $H_2$  production through water splitting, considerable attention has been paid to developing potential semiconductor photocatalysts with high efficiency, chemical stability and response to visible-light irradiation.

“Recently, graphitic carbon nitride (g- $C_3N_4$ ), has emerged as a typical metal-free organic semiconductor photocatalyst for visible light photocatalytic  $H_2$  production via water splitting. Since 2009 [11], g- $C_3N_4$  photocatalyst associated with the unique properties of g- $C_3N_4$ , such as appropriate band gap (~2.7 eV), excellent in physical and chemical stability, abundance and non-toxicity, have been extensively studied”

[12,13]. “However, the photocatalytic performance of the  $H_2$  evolution of pristine g- $C_3N_4$  seems to be limited because of its poor light absorption and the fast recombination rate of photo induced charge carriers” [5]. To overcome these problems, researchers have developed different strategies that improve the photocatalytic efficiency of pure g- $C_3N_4$ , such as doping with metal or non-metal elements [13,14], controlling morphology [1,15] and constructing heterojunctions with other semiconductors [5,7,12].

“Constructing heterojunctions between g- $C_3N_4$  photocatalysts and other materials has been identified as the most effective and feasible route for the improvement of charge migration and separation in g- $C_3N_4$ ” [5,7,12]. Therefore, g- $C_3N_4$  can be merged with a suitable material to form a g- $C_3N_4$ -based heterostructure photocatalyst for  $H_2$  production. Various cobalt-based compounds, such as CoO [16],  $Co_3N$  [17] and  $Co(OH)_2$  [18] are widely used as effective catalysts for constructing g- $C_3N_4$ -based composite photocatalysts and show outstanding performance in photocatalytic  $H_2$  evolution reactions. Ternary cobalt-based catalyst (CoBP) has been found to intensify significant attention in the electrocatalysis studies of  $H_2$  production enhanced by its synergistic effect of elements P and B [19–21]. For example, Hongming Sun *et al.* [19] synthesized CoBP nanosheets supported on a Ni foam; the nanosheets were showed remarkably enhanced electrocatalytic activity in  $H_2$  evolution. Chunduri *et al.* [20] synthesized an amorphous CoBP bifunctional electrocatalyst to enhance alkaline water splitting in electrocatalytic

H<sub>2</sub> production reaction. Thus, a more efficient g-C<sub>3</sub>N<sub>4</sub>-composite can be designed according to CoBP catalyst to enhance the photocatalytic performance of H<sub>2</sub> production. However, the synthesis of C<sub>3</sub>N<sub>4</sub>/CoBP nanocomposite photocatalyst for photocatalytic H<sub>2</sub> production through water splitting under visible-light irradiation has not been reported.

The present study is the first to report a novel C<sub>3</sub>N<sub>4</sub>/CoBP nanocomposite photocatalyst by decorating an amorphous CoBP on the surface of a g-C<sub>3</sub>N<sub>4</sub> photocatalyst via a simple ultrasonic process. The obtained C<sub>3</sub>N<sub>4</sub>/CoBP nanocomposite photocatalyst showed higher photocatalytic activity and stability for H<sub>2</sub> evolution under visible-light irradiation than pure g-C<sub>3</sub>N<sub>4</sub>. The maximum H<sub>2</sub> evolution rate was obtained after 5 wt% amorphous CoBP was loaded on the surface of g-C<sub>3</sub>N<sub>4</sub> and reached a rate of 51.68 μmol h<sup>-1</sup>, which was 3.8 times that of pure g-C<sub>3</sub>N<sub>4</sub>. The heterojunction formed between the planar aromatic structure g-C<sub>3</sub>N<sub>4</sub> and CoBP molecule accelerated interfacial charge migration and separation. Consequently, the C<sub>3</sub>N<sub>4</sub>/CoBP nanocomposite photocatalyst exhibited significantly high photocatalytic activity for H<sub>2</sub> production. Therefore, merging CoBP with g-C<sub>3</sub>N<sub>4</sub> is a promising method for developing efficient and low-cost photocatalysts for H<sub>2</sub> production through water splitting. This work can provide novel insights into the planning, design and development of efficient photocatalysts with high activity for solar energy applications.

## 2. MATERIALS AND METHODS

### 2.1 Chemicals

Urea (≥ 99 %), cobalt (II) chloride hexahydrate (CoCl<sub>2</sub>.6H<sub>2</sub>O), ammonium chloride (NH<sub>4</sub>Cl), ammonia solution, sodium hypophosphite monohydrate (NaH<sub>2</sub>PO<sub>2</sub>.H<sub>2</sub>O), sodium hydroxide (NaOH), anhydrous sodium sulfate (Na<sub>2</sub>SO<sub>4</sub>), triethanolamine (TEOA, ≥ 78 %), methanol (≥ 99%), lactic acid (≥ 85%) and ascorbic acid (≥ 99%) were purchased from Sinopharm Chemical Reagent Co., Ltd. Sodium borohydride (NaBH<sub>4</sub>) and Chloroplatinic acid hexahydrate (H<sub>2</sub>PtCl<sub>6</sub>.6H<sub>2</sub>O, ≥ 37 % Pt basis) were bought from Aldrich. All chemicals were of analytical grade and used as received from the manufactures without any purification. Double distilled water was produced from a SZ-93A auto-double distillation apparatus (Ya Rong Corp., Shanghai, China).

## 2.2 Preparation of the Photocatalyst

### 2.2.1 Preparation of g-C<sub>3</sub>N<sub>4</sub>

Firstly, 10.0 g of urea was added into covered alumina crucible and calcined at 550 °C for 4 h in a muffle furnace under air atmosphere, at the heating rate of 5 °C min<sup>-1</sup>. After 4 h, the sample was left to cool naturally to room temperature, yellow powder (g-C<sub>3</sub>N<sub>4</sub>) was collected for further use.

### 2.2.2 Preparation of amorphous CoBP

CoBP was prepared by a modified electroless deposition method [19]. In a typical synthesis, solution A containing a 50 mL of aqueous solution of CoCl<sub>2</sub>.6H<sub>2</sub>O (3.5 mmol), NH<sub>4</sub>Cl (25 mmol) and some amount of NH<sub>3</sub>.H<sub>2</sub>O (for adjusting pH to 9), was deaerated and flushed with argon. Meanwhile, a solution B containing a 50 mL of aqueous solution of NaBH<sub>4</sub> (35 mmol), NaH<sub>2</sub>PO<sub>2</sub>.H<sub>2</sub>O (500 mmol) and NaOH (3.8 mmol) which was also deaerated and flushed with argon. Then, solution B was added drop wise to solution A under ultrasonification in an ice bath (ultrasonification was applied throughout the reaction process). Vigorous frothing occurred and a dark product was formed. After the completion of the reaction, the sample was centrifuged and washed thoroughly with distilled water and dried at 50 °C under vacuum, and the corresponding sample was labelled Co-B-P.

### 2.2.3 Preparation of g-C<sub>3</sub>N<sub>4</sub>/CoBP composite photocatalyst

The C<sub>3</sub>N<sub>4</sub>/CoBP composite photocatalyst was obtained by mixing an appropriate amount of g-C<sub>3</sub>N<sub>4</sub> and CoBP in solution and then was placed in ultrasonic bath for 3 h, followed by drying for the removal of solvent.

## 2.3 Characterization

“The crystal phase of the samples were characterized by powder X-ray diffraction (XRD) measurements using X-ray diffractometer (MXPAHF, Japan) with Cu K $\alpha$  irradiation ( $\lambda$  = 1.541 Å) at operating voltage of 40 kV and a current of 200 mA. Morphology of the photocatalysts was confirmed by Transmission electron microscopy (TEM) on JEOL-2010, Japan) at accelerating voltage of 200 kV. The XPS was recorded to study the elemental composition and binding energies of the sample and operated by ESCALAB 250 high-

performance electron spectrometer which was set to monochromated Al K $\alpha$  radiation as the excitation source. The UV-vis diffuse reflectance spectra of the photocatalysts were recorded by a Shimadzu spectrophotometer (Model 2501 PC). The steady-state photoluminescence (PL) spectra were conducted on a fluorescence spectrophotometer (JY Fluorolog-3-Tau) with the excitation wavelength at 325 nm. The time-resolved photoluminescence (TRPL) was measured on a Laser Strobe Time-Resolved Spectrofluorometer (Photon Technology International (Canada) Inc.) with a USHIO xenon lamp source, a GL-302 high-resolution dye laser (lifetimes 100 ps to 50 ms, excited by a Nitrogen laser) and a 914 photomultiplier detection system”.

## 2.4 Photoelectrochemical Measurements

“Photoelectrochemical tests were carried out at CHI 760E electrochemical workstation (Chenhua Instrument Company, Shanghai, China) based on a standard three-electrode system, composed of Ag/AgCl as the reference electrode, Pt wire as the counter electrode and indium-tin oxide (ITO) glass as the working electrode. Na<sub>2</sub>SO<sub>4</sub> (0.5 M) was used as the electrolyte solution. A 300 W Xe lamp was used as a solar light source ( $\lambda \geq 420$  nm). For the preparation of working electrodes, 2 mg of either g-C<sub>3</sub>N<sub>4</sub> or C<sub>3</sub>N<sub>4</sub>/5 wt% CoBP samples was dispersed in 1 mL ethanol and 10  $\mu$ L Nafion solution by ultrasonification process. The resulting dispersion was spin-coated onto a piece of ITO glass with a fixed area of ca. 1 cm<sup>2</sup> and annealed at 300 °C for 2 h to remove the organic species completely. The amperometric photocurrents were measured for each switch on/off event with a bias voltage of 0.5 V under visible light irradiation. The electrochemical impedance spectroscopy (EIS) was recorded under visible light and a bias of -1 V and the frequency range was from 10 mHz to 100 kHz in parallel to an alternating current signal amplitude of 5 mV”.

## 2.5 Photocatalytic Hydrogen Production Test

“The photocatalytic hydrogen evolution from water splitting was carried out in an outer Pyrex top-irradiation reaction vessel (500 mL) connected to a glass closed gas circulation system. In a typical experiment, 10 mL of triethanolamine (TEOA) was used as a sacrificial agent in an aqueous solution of 100 mL. 50 mg of g-C<sub>3</sub>N<sub>4</sub> powder and CoBP with different

amounts were dispersed in water and then kept in an ultrasonic bath for half an hour. Then, 1 wt% Pt, as a co-catalyst to boost H<sub>2</sub> generation was loaded onto the surface of the catalyst by in situ photodeposition method using H<sub>2</sub>PtCl<sub>6</sub>.6H<sub>2</sub>O. In order to make sure anaerobic conditions in the reaction system, the solution was evacuated 1 h to remove air completely before irradiation by a 300 W xenon lamp (Perfect Light, PLS-SXE300C, Beijing). The xenon lamp is equipped with a cut-off filter ( $\lambda \geq 420$  nm) to remove ultraviolet light. Besides, the Pyrex reactor with a double layer was continuously stirred, and a flow of cooling ethylene glycol was used during the photocatalytic reaction to maintain the temperature of the reaction solution at 10 °C. The amount of hydrogen evolution from photocatalytic splitting water was measured using on-line gas chromatography (GC1120, Shanghai Sunny Hengping Limited, HTCD, nitrogen as carrier gas). After the reaction, the photocatalysts were separated from the reaction solution for further characterization. The catalysts are denoted as C<sub>3</sub>N<sub>4</sub>/x CoBP, where x (x = 4, 5, 6 %) refers to the weight content of CoBP in C<sub>3</sub>N<sub>4</sub>/CoBP samples”.

The apparent quantum yield (AQY) was measured under different monochromatic light irradiation by using C<sub>3</sub>N<sub>4</sub>/5 wt% CoBP photocatalyst (irradiated by a 300 W Xe lamp using the bandpass filter of  $\lambda \pm 5$  nm for 420, 450, 500, 550, 600 nm), and was calculated according to the equation given below:

$$\begin{aligned} \text{AQY (\%)} &= \frac{\text{Number of reacted electrons}}{\text{Number of incident photons}} \times 100\% \\ &= \frac{\text{Number of evolved H}_2 \text{ molecules} \times 2}{\text{Number of incident photons}} \times 100\% \end{aligned}$$

## 3. RESULTS AND DISCUSSION

Graphitic carbon nitride (g-C<sub>3</sub>N<sub>4</sub>) was prepared from urea and calcined at 550 °C for 4 h, CoBP molecule was synthesised by an electroless deposition method (Fig. S1) and g-C<sub>3</sub>N<sub>4</sub>/CoBP nanocomposite photocatalysts were obtained by mixing g-C<sub>3</sub>N<sub>4</sub> and CoBP in a solution and then dried. The X-ray diffraction (XRD) patterns of the samples prepared are displayed in Fig. 1a. Pure g-C<sub>3</sub>N<sub>4</sub> exhibited two main diffraction peaks with different intensities. The low-angle diffraction peak at 13.0° index was attributed to the (100) plane, and the high-angle diffraction peak at 27.7° was attributed to the (002) lattice plane. These arrangements reflected an in-plane structural packing motif of a tri-s-triazine unit and

the interlayer stacking peak of conjugated aromatic systems observed for g-C<sub>3</sub>N<sub>4</sub>, respectively [6,22]. The XRD patterns of composite C<sub>3</sub>N<sub>4</sub>/CoBP with 5 wt% CoBP displayed similar diffraction peaks observed on the original g-C<sub>3</sub>N<sub>4</sub>. Remarkably, no other impurity phase was observed. The well-crystal structure of g-C<sub>3</sub>N<sub>4</sub> was not affected by CoBP loading. In addition, no intense diffraction peaks were observed in the XRD pattern of pure CoBP confirming noncrystallinity, and only a single broad peak was detected (at approximately 45°; Fig. 1b), indicating the amorphous structure of CoBP [19,23,24]. In addition, EDS measurement of CoBP molecule was performed and the spectrum (Fig. S2) confirmed the existence of only Co, B, and P in the molecule.

The prepared CoBP molecule displayed a nanosphere morphology (Fig. 2a). However, after 5 wt% CoBP was loaded, the morphology of the composite photocatalyst C<sub>3</sub>N<sub>4</sub>/CoBP remained unchanged in contrast to the morphology of g-C<sub>3</sub>N<sub>4</sub>. This result demonstrated that CoBP did not affect the morphology of the g-C<sub>3</sub>N<sub>4</sub> photocatalyst (Fig. 2b and c). The high-resolution TEM and selected area electron diffraction (SAED) images of CoBP were used in verifying the amorphous nature of CoBP. The HR-TEM image did not indicate the presence of any crystalline phase or lattice plane (Fig. 2d). This result was confirmed by the occurrence of diffused rings in the SAED image (inset of Fig. 2d) [19–21].

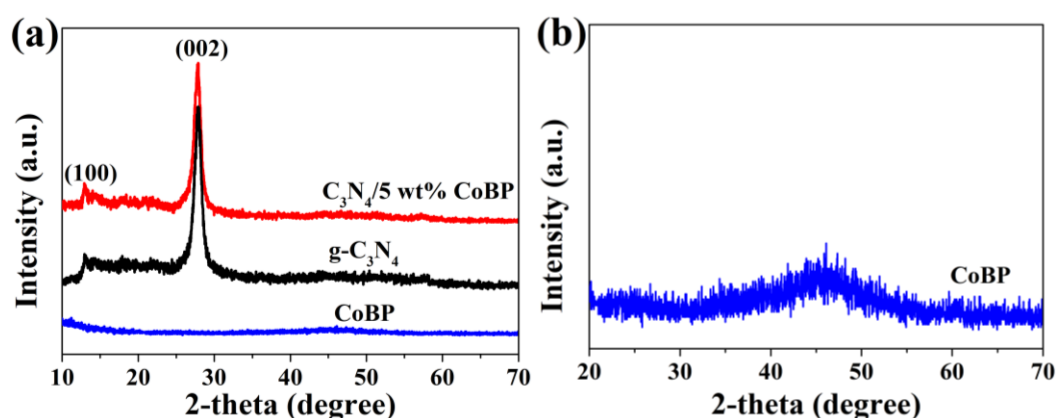


Fig. 1. (a) XRD patterns of CoBP molecule, g-C<sub>3</sub>N<sub>4</sub> and C<sub>3</sub>N<sub>4</sub>/5 wt% CoBP photocatalysts. (b) XRD patterns of amorphous CoBP

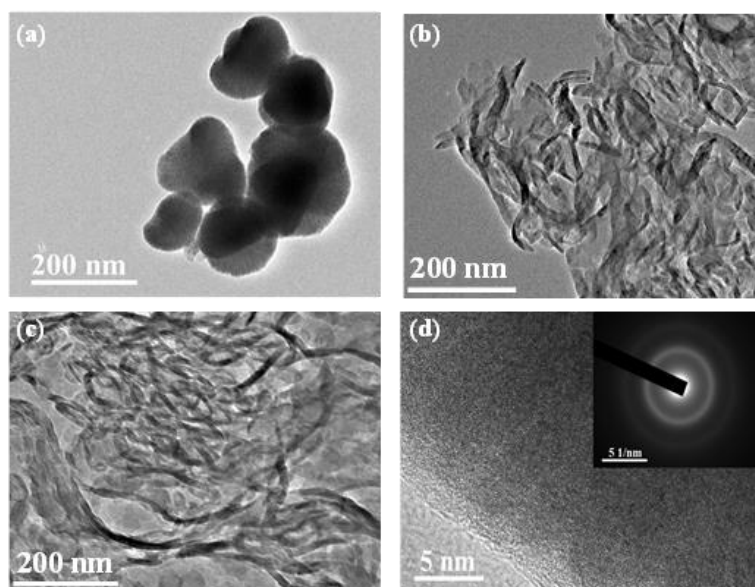


Fig. 2. TEM images of (a) CoBP sample, (b) Pure g-C<sub>3</sub>N<sub>4</sub>, (c) g-C<sub>3</sub>N<sub>4</sub> /5 wt% CoBP photocatalysts. (d) HR-TEM image and SAED pattern (inset) of CoBP sample

To investigate the chemical states of the prepared CoBP catalyst, an X-ray photoelectron spectroscopy (XPS) test was carried out (Fig. S3). The XPS spectrum of the Co 2p (Fig. S3a) displayed two major peaks. “A strong peak was detected at a binding energy 780.7 eV for Co 2p<sub>3/2</sub>, and a minor peak at 796.5 eV for Co 2p<sub>1/2</sub>. In addition, two satellite peaks were detected in the Co 2p spectra at binding energy of 786.5 and 802.96 eV, confirming the presence of elemental Co and the oxidised state of Co in the catalyst” [19–21,25]. The peaks of boron 1s were detected in the high-resolution XPS spectrum at 188.0 and 190.33 eV, which were attributed to boron in elemental and oxidised states, respectively (Fig. S3b). The binding energy of elemental boron shifted positively by 0.8 eV compared with the reported binding energy of pure boron (187.2 eV) [19,25]. “With respect to P 2p high-resolution XPS spectrum (Fig. S3c), phosphorous showed two distinct peaks at 129.5 and 132.83 eV, which might be assigned to the presence of P<sup>o</sup> and oxidised phosphorous species, respectively” [19–21,25].

In general, the photocatalytic activity of H<sub>2</sub> production through water splitting depended on the optical absorption efficiency of catalysts and can be employed to determine the band gap of semiconductor photocatalyst. The UV–visible (UV–vis) diffuse reflectance spectra of CoBP, g-C<sub>3</sub>N<sub>4</sub> and C<sub>3</sub>N<sub>4</sub>/5 wt% CoBP composite photocatalyst were collected to show their optical properties. As shown in Fig. 3a, bare g-C<sub>3</sub>N<sub>4</sub> absorbed visible light with absorption edge of approximately 450 nm (band gap of ~2.7 eV) because of the excitation of electrons from the valence band to the conduction band [5]. After 5 wt% CoBP was loaded, the composite C<sub>3</sub>N<sub>4</sub>/CoBP showed an absorption edge nearly

similar to that of pure g-C<sub>3</sub>N<sub>4</sub>, confirming that no structural change occurred in g-C<sub>3</sub>N<sub>4</sub>. Additionally, the absorption intensity of g-C<sub>3</sub>N<sub>4</sub> slightly increased after the loading of 5 wt% CoBP, showing that CoBP was successfully introduced to the surface of g-C<sub>3</sub>N<sub>4</sub>. Based on the UV-vis spectra, the optical band gap value of CoBP was calculated from the Kubelka–Munk method (Fig. 3b) and determined to be approximately 1.59 eV.

“To explore the migration, the transfer and separation of the photogenerated electron–hole pairs over g-C<sub>3</sub>N<sub>4</sub> and C<sub>3</sub>N<sub>4</sub>/5 wt% CoBP samples, the steady-state photoluminescence (PL) and time-resolved photoluminescence (TRPL) spectra were recorded. As displayed in Fig. 4a, the PL emission peak of pure g-C<sub>3</sub>N<sub>4</sub> centered at approximately 450 nm under an excitation wavelength of 325 nm at room temperature, resulting from the electron–hole recombination in g-C<sub>3</sub>N<sub>4</sub>” [6,26]. “The C<sub>3</sub>N<sub>4</sub>/5 wt% CoBP composite displayed an emission peak similar to that of pure g-C<sub>3</sub>N<sub>4</sub>, but the peak intensity significantly declined because of the effective suppression of photogenerated charge carriers. Thus, photocatalytic activity for H<sub>2</sub> production was boosted. The charge transfer efficiency within the composite was measured, and the results are shown in Fig. 4b. The average lifetimes of the photogenerated charge carriers for g-C<sub>3</sub>N<sub>4</sub> and C<sub>3</sub>N<sub>4</sub>/5 wt% CoBP samples were 2.54 ± 0.21 and 3.11 ± 0.26 ns, respectively. Long lifetimes are ascribed to the rapid transfer and separation of photogenerated charge carriers and subsequent inhibition of recombination” [6,22]. This result confirmed that loading a suitable amount of CoBP induces charge transfer and thereby significantly increase H<sub>2</sub> production rate.

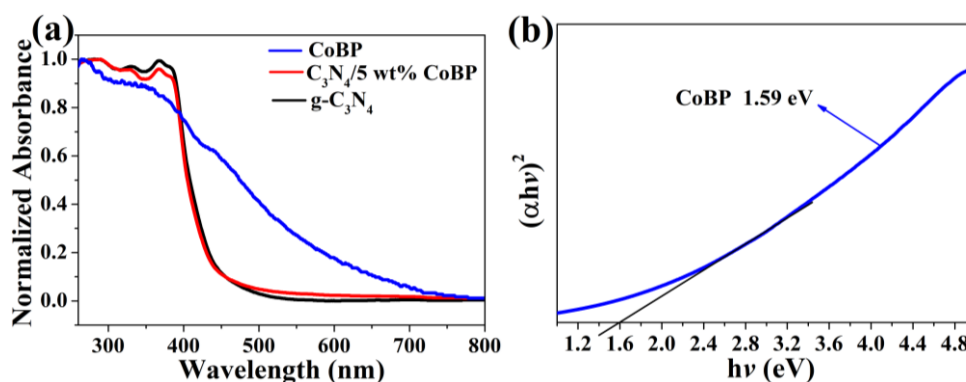


**Fig. 3. (a)** The diffuse reflectance UV-vis absorption spectra of solid CoBP molecule, g-C<sub>3</sub>N<sub>4</sub> and C<sub>3</sub>N<sub>4</sub>/5 wt% CoBP photocatalysts. **(b)** Band gap evaluation from the plots of  $(\alpha h\nu)^2$  vs the energy of the absorbed light of the NPBI molecule



“Moreover, photoelectrochemical tests over  $g\text{-C}_3\text{N}_4$  and  $\text{C}_3\text{N}_4/5\text{ wt\% CoBP}$  samples were performed under visible-light irradiation ( $\lambda \geq 420\text{ nm}$ ) to investigate the effect of CoBP on the generation and migration of photogenerated charge carriers. As shown in Fig. 4c, under several on–off visible-light irradiation cycles of a photocurrent response, both electrodes generated rapid and constant photocurrent responses. Compared with the pure  $g\text{-C}_3\text{N}_4$  photocatalyst,  $\text{C}_3\text{N}_4/5\text{ wt\% CoBP}$  composite photocatalyst showed stable and higher photocurrent density (nearly twofold that of pure  $g\text{-C}_3\text{N}_4$ ). The high photocurrent responses of  $\text{C}_3\text{N}_4/5\text{ wt\% CoBP}$  hybrid indicated efficient charge migration and separation between  $g\text{-C}_3\text{N}_4$  and CoBP interfaces” [5,17]. “This observation is a good indicator of the inhibited recombination of photogenerated electron and holes. This effect was in a good agreement with the results of PL spectra. In addition, the electrochemical impedance spectroscopy (EIS) test of  $g\text{-C}_3\text{N}_4$  and  $\text{C}_3\text{N}_4/5\text{ wt\% CoBP}$  was performed at an alternating current voltage of 0.5 V to study charge transfer resistance. As displayed in Fig. 4d, the  $\text{C}_3\text{N}_4/5\text{ wt\% CoBP}$  sample exhibited a smaller arc radius than pure  $g\text{-C}_3\text{N}_4$ , implying efficient charge migration and separation, both of

which are beneficial for the photocatalytic performance of  $\text{H}_2$  production” [17,27]. The obtained Nyquist plots data were fitted with the Randles circuit (Fig. 4d inset, where  $R_s$  and  $R_{ct}$  represent solution resistance and charge transfer resistance between the electrolyte and electrode, respectively). The EIS-fitted parameters are displayed in Table S1 in Supporting Information. The results of photoelectrochemical tests showed that charge migration and separation indeed occurred at the interface between  $g\text{-C}_3\text{N}_4$  and CoBP.

To compare the photocatalytic activity of  $\text{H}_2$  evolution over different prepared photocatalysts, a series of comparative experiments were performed. Firstly, the  $\text{H}_2$  evolution rate was measured by using different sacrificial agents under visible-light irradiation ( $\lambda \geq 420\text{ nm}$ ). As shown in Fig. S4, the  $\text{C}_3\text{N}_4/5\text{ wt\% CoBP}$  composite photocatalyst exhibited a high  $\text{H}_2$  evolution rate when triethanolamine (TEOA) was used as the sacrificial agent in the photocatalytic reaction. TEOA is suitable at high  $\text{H}_2$  level because of its high redox potential and the created basic environment [28]. Thus TEOA was considered the best sacrificial agent.

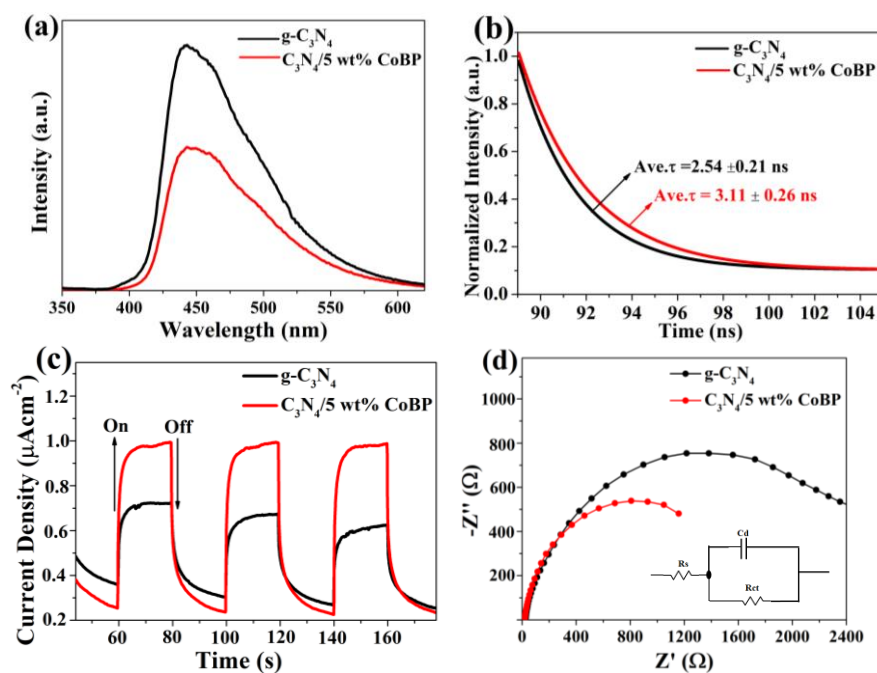


**Fig. 4.** (a) Steady-state photoluminescence spectra. (b) Time-resolved fluorescence decay traces for  $g\text{-C}_3\text{N}_4$  and  $\text{C}_3\text{N}_4/5\text{ wt\% CoBP}$  photocatalyst (excitation at 325 nm, emission at 450 nm). (c) Transient photocurrent response. (d) EIS Nyquist plots for  $g\text{-C}_3\text{N}_4$  and  $\text{C}_3\text{N}_4/5\text{ wt\% CoBP}$  under visible light irradiation ( $\lambda \geq 420\text{ nm}$ ,  $[\text{Na}_2\text{SO}_4] = 0.5\text{ M}$ ). The inset correspond to the fitting using the equivalent circuit

Furthermore, the H<sub>2</sub> evolution rate over different samples were measured under visible-light irradiation (Fig. 5). The sample of g-C<sub>3</sub>N<sub>4</sub> with 1 wt% Pt cocatalyst (Fig. 5b) displayed high photocatalytic activity (13.47 μmol h<sup>-1</sup>) compared with pure g-C<sub>3</sub>N<sub>4</sub> (Fig. 5a) due to the fast recombination rate of photogenerated electron-hole pairs. The visible photocatalytic H<sub>2</sub> evolution rate of g-C<sub>3</sub>N<sub>4</sub> significantly increased up to 51.68 μmol h<sup>-1</sup> when 5 wt% CoBP was added (Fig. 5c). This value was 3.8 times that of pure g-C<sub>3</sub>N<sub>4</sub>. To confirm the role of CoBP in the photocatalytic system, the H<sub>2</sub> evolution rate of C<sub>3</sub>N<sub>4</sub>/5 wt% CoBP without deposition of Pt cocatalyst was 5.31 μmol h<sup>-1</sup> (Fig. 5d). A controlled experiment was then performed for a pure CoBP sample. The results demonstrated that no hydrogen evolution occurred when only pure CoBP was used as the photocatalyst. These results showed that enhanced photocatalytic activity can be attributed to the formation of heterojunction in the C<sub>3</sub>N<sub>4</sub>/CoBP composite photocatalyst. The heterojunction facilitated charge transfer and separation, which in turn improved photocatalytic activity during H<sub>2</sub> evolution.

Moreover, the photocatalytic H<sub>2</sub> evolution rates of g-C<sub>3</sub>N<sub>4</sub> at different amounts of CoBP (4, 5 and 6 wt%) were further investigated under visible-light

irradiation ( $\lambda \geq 420$  nm). TEOA was used as the sacrificial reagent (Fig. 6a). The introduction of CoBP greatly improved photocatalytic H<sub>2</sub> evolution rate. Pure g-C<sub>3</sub>N<sub>4</sub> exhibited the extremely low photocatalytic activity of H<sub>2</sub> evolution rate (13.47 μmol h<sup>-1</sup>). When 4 wt% CoBP was introduced, the H<sub>2</sub> evolution rate increased up to 36.37 μmol h<sup>-1</sup>. Remarkably, when 5 wt% CoBP was loaded, the H<sub>2</sub> evolution rate further increased and reached a maximum value of 51.68 μmol h<sup>-1</sup>, which was 3.8 that of bare g-C<sub>3</sub>N<sub>4</sub>. This value was higher than the maximum values of other g-C<sub>3</sub>N<sub>4</sub>-based heterostructure photocatalysts (Table S2) [6,16,29,30]. As CoBP loading further increased to 6 wt%, the H<sub>2</sub> evolution rate decreased to 39.77 μmol h<sup>-1</sup>. The possible reasons were as follows: (i) the black color of CoBP led to a significant increase in opacity and shielding effect that prevented incident light from reaching the surface of the g-C<sub>3</sub>N<sub>4</sub> photocatalyst and (ii) an excessive amount of CoBP blocked active sites on the surface of g-C<sub>3</sub>N<sub>4</sub> and impeded contact between the reactive sites and reactants [6,13]. Thus, loading a suitable amount of CoBP onto g-C<sub>3</sub>N<sub>4</sub> is a suitable method for increasing photocatalytic activity in the H<sub>2</sub> evolution of C<sub>3</sub>N<sub>4</sub>/CoBP composite photocatalysts.

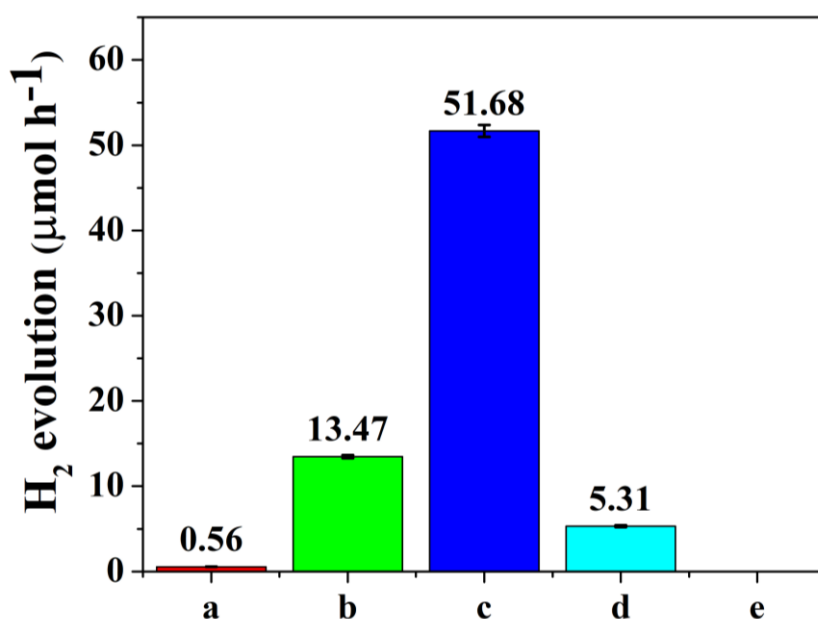


**Fig. 5.** Comparison of H<sub>2</sub> evolution rates over different samples; (a) g-C<sub>3</sub>N<sub>4</sub> without the Pt cocatalyst, (b) g-C<sub>3</sub>N<sub>4</sub> with 1% Pt, (c) C<sub>3</sub>N<sub>4</sub>/5 wt% CoBP with 1% Pt cocatalyst, (d) C<sub>3</sub>N<sub>4</sub>/5 wt% CoBP without the Pt cocatalyst, (e) CoBP alone without Pt cocatalyst: Reaction conditions: 50 mg of photocatalyst,  $\lambda \geq 420$  nm, 100 mL of solvent, H<sub>2</sub>O/TEOA = 9:1 (vol/vol), light source, xenon lamp (300 W) with a cutoff filter; temperature, 10 °C



To test the reciprocal effects of Pt loading amount, we measured the activity of  $C_3N_4/5$  wt% CoBP catalysts with varied wt% Pt loading content (Fig. S5). The surface area of a catalyst plays a vital role in the enhancement of photocatalytic activity of a catalyst. Catalysts with large specific surface areas have numerous active sites that improve light absorption [29]. Nitrogen sorption isotherms were measured to determine the specific surface areas of the prepared catalysts. As shown in Fig. S6, the BET specific surface areas ( $S_{BET}$ ) of pure  $g-C_3N_4$  and  $C_3N_4/5$  wt% CoBP composite were 89 and 114  $m^2g^{-1}$ , respectively. The composite photocatalyst showed higher  $S_{BET}$  than pure  $g-C_3N_4$  because of the insertion of CoBP, and the addition of CoBP increased the surface area of the composite catalyst. This effect enhanced the performance of  $C_3N_4/5$  wt% CoBP for  $H_2$  production.

Furthermore, to confirm that the photocatalytic activity of  $H_2$  evolution is dependent on light absorption of a catalyst, the apparent quantum yield (AQY) of  $H_2$  evolution of  $C_3N_4/5$  wt% CoBP was measured under the same reaction conditions but different levels of monochromatic light irradiation ( $\lambda \pm 5$  nm for 420, 450, 500, 550 and 600 nm). The AQYs varied inversely with the UV-vis absorption spectrum of  $C_3N_4/5$  wt% CoBP composite photocatalyst (Fig. 6b). Notably, the harvested visible photons dominated the driving force for the photocatalytic  $H_2$  evolution reactions.[6] Interestingly, our  $C_3N_4/CoBP$  composite photocatalyst exhibited AQY of approximately 5.42% at 420 nm, which was higher than the AQYs other  $g-C_3N_4$ -based heterostructure photocatalysts (Table S2) [6,30,31].

Apart from the photocatalytic performance of  $H_2$  evolution, an ideal photocatalyst must have photocatalytic stability and can be recycled for large-scale practical applications. To investigate photocatalytic stability, the  $C_3N_4/5$  wt% CoBP composite photocatalyst was subjected to a recycling test involving five consecutive cycles of photocatalytic activity of  $H_2$  evolution under the same experimental conditions (Fig. 7). No obvious loss of  $H_2$  evolution activity was observed in the  $C_3N_4/5$  wt% CoBP sample after 20 h of illumination, and the amount of  $H_2$  evolved was nearly the same as that of the first cycle, implying that the composite photocatalyst exhibited good stability for photocatalytic  $H_2$  production under prolonged visible-light irradiation. The XRD patterns of the  $C_3N_4/5$  wt% CoBP composite photocatalyst before and after the recycling tests are shown in Fig. S7. No obvious change was observed in the  $C_3N_4/5$  wt% CoBP composite before and after recycling. Overall, the findings of this study indicated the stability of the  $C_3N_4/5$  wt% CoBP composite photocatalyst during the photocatalytic  $H_2$  evolution. Therefore, the composite can be reused in photocatalytic reactions.

The results demonstrated that CoBP plays a crucial role in the separation and migration of electron-hole pairs in  $C_3N_4/CoBP$  hybrid photocatalysts. This role benefits from the formation of a heterojunction between amorphous CoBP molecule and  $g-C_3N_4$  nanosheet photocatalyst. The CB and VB energy levels of  $g-C_3N_4$  are -1.12 and +1.57 eV (vs. NHE), respectively [32–34]. The CB and VB of CoBP were estimated using valence band X-ray photoelectron spectroscopy (VB-XPS) and UV–

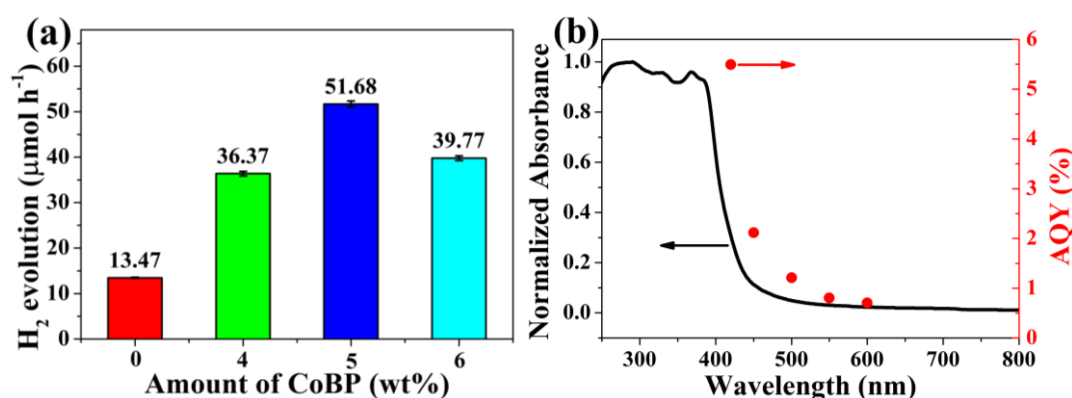


**Fig. 6. (a) Comparison of the photocatalytic activity of  $C_3N_4/CoBP$  catalysts with different weight of CoBP, 1 wt% Pt as cocatalyst. (b) Wavelength-dependent apparent quantum yield (AQY) relationship for the photocatalytic hydrogen evolution**

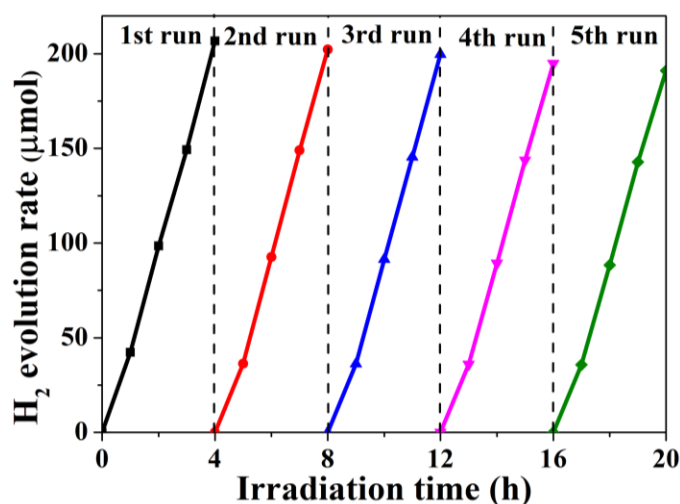


**Fig.7.** The reusability tests of C<sub>3</sub>N<sub>4</sub>/5 wt% CoBP with 1 % Pt cocatalyst for photocatalytic hydrogen production. Reaction conditions: 50 mg of photocatalyst, solvent [100 mL, H<sub>2</sub>O/TEOA = 9:1 (vol/vol)] and a 300 W Xenon lamp as light source equipped with a cut-off filter ( $\lambda \geq 420$  nm), at 10 °C, and H<sub>2</sub> produced was evacuated after every 4 h

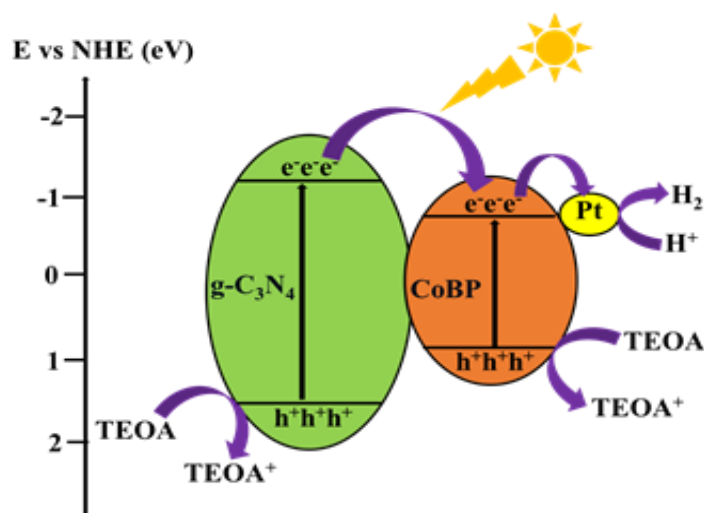


**Fig. 8.** Proposed mechanism of electron–hole transport process and photocatalytic activity of C<sub>3</sub>N<sub>4</sub>/CoBP heterostructure photocatalyst under visible-light irradiation

vis diffuse reflection spectra. As displayed in Fig. S8, the VB edge position of CoBP was 0.89 eV, and the CB was -0.7 eV. These findings suggested a possible mechanism for visible-light-induced H<sub>2</sub> production activity in the C<sub>3</sub>N<sub>4</sub>/CoBP composite (Fig. 8). The CB edge position of g-C<sub>3</sub>N<sub>4</sub> was more negative than that of CoBP, and thus CoBP acted as an outstanding electron sink. These electrons were then transported to Pt nanoparticle to prolong the lifetime of charge carriers (Fig. 8). The remaining holes in the VB of g-C<sub>3</sub>N<sub>4</sub> and CoBP were consumed by the sacrificial electron donor (TEOA; Fig. 8). Overall, CoBP served as a charge-separation centre that

restrained the recombination of photogenerated electrons and holes in g-C<sub>3</sub>N<sub>4</sub> and significantly improved the photocatalytic activity for H<sub>2</sub> production.

#### 4. CONCLUSION

A novel type of C<sub>3</sub>N<sub>4</sub>/CoBP composite photocatalyst was successfully fabricated by decorating CoBP on the surface of g-C<sub>3</sub>N<sub>4</sub> through ultrasonication. The formation of a heterojunction between g-C<sub>3</sub>N<sub>4</sub> and CoBP facilitated the migration and separation of photogenerated charge carriers in the system.

Therefore, the C<sub>3</sub>N<sub>4</sub>/CoBP hybrid photocatalyst exhibited a higher level of photocatalytic activity for H<sub>2</sub> evolution than pure g-C<sub>3</sub>N<sub>4</sub> under visible-light irradiation ( $\lambda \geq 420$  nm). Excellent charge transfer and separation led to a dramatic improvement in H<sub>2</sub> evolution rate, which reached up to 51.60  $\mu\text{mol h}^{-1}$  under 5 wt% CoBP. This rate was 3.8 times that of bare g-C<sub>3</sub>N<sub>4</sub> (13.47  $\mu\text{mol h}^{-1}$ ) and corresponded to an AQY of 5.42 % at 420 nm. Notably, the C<sub>3</sub>N<sub>4</sub>/CoBP composite photocatalyst displayed excellent photocatalytic stability and reusability for H<sub>2</sub> evolution after 20 h of irradiation. The CoBP is a promising material that combines with the low-cost g-C<sub>3</sub>N<sub>4</sub> to form a C<sub>3</sub>N<sub>4</sub>/CoBP hybrid for practical use in photocatalytic H<sub>2</sub> production. In conclusion, this work offers a simple method for designing and developing not only highly efficient but also stable heterostructured photocatalysts for solar-to-chemical energy conversion.

### COMPETING INTERESTS

Authors have declared that no competing interests exist.

### REFERENCES

- Ling GZS, Oh VBY, Haw CY, Tan LL, Ong WJ. g-C<sub>3</sub>N<sub>4</sub> Photocatalysts: Utilizing Electron–Hole Pairs for Boosted Redox Capability in Water Splitting. *Energy Material Advances* 2023;4:1–27. Available: <https://doi.org/10.34133/energymatadv.0038>.
- Ding Q, Zou X, Ke J, Dong Y, Cui Y, Lu G, et al. S-scheme 3D/2D NiCo<sub>2</sub>O<sub>4</sub>@g-C<sub>3</sub>N<sub>4</sub> hybridized system for boosting hydrogen production from water splitting. *Renewable Energy* 2023;203:677–85. Available: <https://doi.org/10.1016/j.renene.2022.12.115>.
- Fujishima A, Honda K. Electrochemical Photolysis of water at a Semiconductor electrode. *Nature* 1972;238:37-38.
- Tahir W, Cheang TY, Li JH, Ling C, Lu XJ, Ullah I, et al. Interfacial Ti  $\equiv$  N bonding of a g-C<sub>3</sub>N<sub>4</sub>/TiH<sub>1.92</sub> type-II heterojunction photocatalyst significantly enhanced photocatalytic hydrogen evolution from water splitting. *Catalysis Science and Technology* 2022;12:2023–9. Available: <https://doi.org/10.1039/d1cy02039k>.
- Kombo M, Chong HB, Ma LB, Sahar S, Fang XX, Zhao T, et al. Graphitic carbon nitride decorated with nickel(II)-(3-Pyridyl) benzimidazole complexes and pt nanoparticles as a cocatalyst for photocatalytic hydrogen production from water splitting. *ACS Applied Nano Materials* 2020;3:10659–67. Available: <https://doi.org/10.1021/acsanm.0c01872>.
- Kombo M, Ma LB, Liu YN, Fang XX, Ullah N, Odda AH, et al. Graphitic carbon nitride/CoTPP type-II heterostructures with significantly enhanced photocatalytic hydrogen evolution. *Catalysis Science and Technology* 2019;9:2196–202. Available: <https://doi.org/10.1039/c9cy00140a>.
- Wang R, Ye C, Wang H, Jiang F. Z-scheme LaCoO<sub>3</sub>/g-C<sub>3</sub>N<sub>4</sub> for efficient full-spectrum light-simulated solar photocatalytic hydrogen generation. *ACS Omega* 2020;5:30373–82. Available: <https://doi.org/10.1021/acsomega.0c03318>.
- Jiang L, Wang K, Wu X, Zhang G, Yin S. Amorphous bimetallic cobalt nickel sulfide cocatalysts for significantly boosting photocatalytic hydrogen evolution performance of graphitic carbon nitride: Efficient interfacial charge transfer. *ACS Applied Materials & Interfaces* 2019;11:26898–908. Available: <https://doi.org/10.1021/acsaami.9b07311>.
- Bai Y, Li C, Liu L, Yamaguchi Y, Bahri M, Yang H, et al. Photocatalytic overall water splitting under visible light enabled by a particulate conjugated polymer loaded with palladium and iridium \*\*. *Angewandte* 2022. Available: <https://doi.org/10.1002/ange.202201299>.
- Novoa-cid M, Melillo A, Alvaro M, Baldovi HG. Photocatalytic water splitting promoted by 2D and 3D porphyrin covalent organic polymers synthesized by Suzuki-Miyaura Carbon-Carbon Coupling; 2022.
- Wang X, Maeda K, Thomas A, Takanabe K, Xin G, Carlsson JM, et al. A metal-free polymeric photocatalyst for hydrogen production from water under visible light. *Nature Materials* 2009;8:76–80. Available: <https://doi.org/10.1038/nmat2317>.
- Tahir W, Ullah S, Ullah I, Li JH, Ling C, Lu XJ, et al. Metallic WN plasmonic fabricated g-C<sub>3</sub>N<sub>4</sub> significantly steered photocatalytic hydrogen evolution under visible and near-infrared light. *Catalysis Science and Technology* 2022;12:7369–78. Available: <https://doi.org/10.1039/d2cy01499h>.

13. Fang XX, Ma LB, Liang K, Zhao SJ, Jiang YF, Ling C, et al. The doping of phosphorus atoms into graphitic carbon nitride for highly enhanced photocatalytic hydrogen evolution. *Journal of Materials Chemistry A* 2019;7:11506–12. Available: <https://doi.org/10.1039/c9ta01646e>.
14. Prasad C, Tang H, Liu Q, Bahadur I, Karlapudi S, Jiang Y. A latest overview on photocatalytic application of g-C<sub>3</sub>N<sub>4</sub> based nanostructured materials for hydrogen production. *International Journal of Hydrogen Energy* 2020;45:337–79. Available: <https://doi.org/10.1016/j.ijhydene.2019.07.070>.
15. Wudil YS, Ahmad UF, Gondal MA, Al-Osta MA, Almohammed A, Sa'id RS, et al. Tuning of graphitic carbon nitride (g-C<sub>3</sub>N<sub>4</sub>) for photocatalysis: A critical review. *Arabian Journal of Chemistry* 2023;16:104542. Available: <https://doi.org/10.1016/j.arabjc.2023.104542>.
16. Mao Z, Chen J, Yang Y, Wang D, Bie L, Fahlman BD. Novel g-C<sub>3</sub>N<sub>4</sub>/CoO Nanocomposites with Significantly Enhanced Visible-Light Photocatalytic Activity for H<sub>2</sub> Evolution. *ACS Applied Materials and Interfaces* 2017;9:12427–35. Available: <https://doi.org/10.1021/acsami.7b00370>.
17. Jin Z, Wei T, Lixue Li, Li F, Tao R, Xu L. Loading Co<sub>3</sub>N nanoparticles as efficient cocatalysts over Zn<sub>0.5</sub>Cd<sub>0.5</sub>S for enhanced H<sub>2</sub> evolution under visible light. *Dalton Transactions* 2019;48:2676–82. Available: <https://doi.org/10.1039/c8dt05087b>.
18. Li Z, Wu Y, Lu G. Highly efficient hydrogen evolution over Co(OH)<sub>2</sub> nanoparticles modified g-C<sub>3</sub>N<sub>4</sub> co-sensitized by Eosin Y and Rose Bengal under Visible Light Irradiation. *Applied Catalysis B: Environmental* 2016;188:56–64. Available: <https://doi.org/10.1016/j.apcatb.2016.01.057>.
19. Sun H, Xu X, Yan Z, Chen X, Jiao L, Cheng F, et al. Superhydrophilic amorphous Co-B-P nanosheet electrocatalysts with Pt-like activity and durability for the hydrogen evolution reaction. *Journal of Materials Chemistry A* 2018;6:22062–9. Available: <https://doi.org/10.1039/C8TA02999G>.
20. Chunduri A, Gupta S, Bapat O, Bhide A, Fernandes R, Patel MK, et al. A unique amorphous cobalt-phosphide-boride bifunctional electrocatalyst for enhanced alkaline water-splitting. *Applied Catalysis B: Environmental* 2019;259:118051. Available: <https://doi.org/10.1016/j.apcatb.2019.118051>.
21. Kim J, Kim H, Kim SK, Ahn SH. Electrodeposited amorphous Co-P-B ternary catalyst for hydrogen evolution reaction. *Journal of Materials Chemistry A* 2018;6:6282–8. Available: <https://doi.org/10.1039/c7ta11033b>.
22. Liu YN, Zhou X, Shen CC, Zhao ZW, Jiang YF, Ma LB, et al. Hydrogen-bonding-assisted charge transfer: Significantly enhanced photocatalytic H<sub>2</sub> evolution over g-C<sub>3</sub>N<sub>4</sub> anchored with ferrocene-based hole relay. *Catalysis Science and Technology* 2018;8:2853–9. Available: <https://doi.org/10.1039/c8cy00488a>.
23. Wang W, Liu P, Wu K, Tan S, Li W, Yang Y. Preparation of hydrophobic reduced graphene oxide supported Ni-B-P-O and Co-B-P-O catalysts and their high hydrodeoxygenation activities. *Green Chemistry* 2016;18:984–8. Available: <https://doi.org/10.1039/c5gc02073e>.
24. Men Y, Su J, Du X, Liang L, Cheng G, Luo W. CoBP nanoparticles supported on three-dimensional nitrogen-doped graphene hydrogel and their superior catalysis for hydrogen generation from hydrolysis of ammonia borane. *Journal of Alloys and Compounds* 2018;735:1271–6. Available: <https://doi.org/10.1016/j.jallcom.2017.11.137>.
25. Jia X, Sang Z, Sun L, Xu F, Pan H, Zhang C, et al. Graphene-Modified Co-B-P Catalysts for Hydrogen Generation from Sodium Borohydride Hydrolysis. *Nanomaterials* 2022;12:1–14. Available: <https://doi.org/10.3390/nano12162732>.
26. Ma LB, Liu YN, Liang K, Fang XX, Sahar S, Kombo M, et al. Hantzsch ester as hole relay significantly enhanced photocatalytic hydrogen production. *Catalysis Science and Technology* 2018;8:6123–8. Available: <https://doi.org/10.1039/c8cy01922c>.
27. Zhu X, Yu S, Gong X, Xue C. In Situ Decoration of Zn<sub>x</sub>Cd<sub>1-x</sub>S with FeP for

- Efficient Photocatalytic Generation of Hydrogen under Irradiation with Visible Light. *ChemPlusChem* 2018;83:825–30. Available: <https://doi.org/10.1002/cplu.201800316>.
28. Wang DH, Pan JN, Li HH, Liu JJ, Wang YB, Kang LT, et al. A pure organic heterostructure of  $\mu$ -oxo dimeric iron(III) porphyrin and graphitic- $C_3N_4$  for solar  $H_2$  production from water. *Journal of Materials Chemistry A* 2015;4:290–6. Available: <https://doi.org/10.1039/c5ta07278f>.
29. Wang W, Liu S, Nie L, Cheng B, Yu J. Enhanced photocatalytic  $H_2$  production activity of  $TiO_2$  using  $Ni(NO_3)_2$  as an additive. *Physical Chemistry Chemical Physics* 2013;15:12033–9. Available: <https://doi.org/10.1039/c2cp43628k>.
30. Ye R, Fang H, Zheng YZ, Li N, Wang Y, Tao X. Fabrication of  $CoTiO_3/g-C_3N_4$  Hybrid Photocatalysts with Enhanced  $H_2$  Evolution: Z-Scheme Photocatalytic Mechanism Insight. *ACS Applied Materials and Interfaces* 2016;8:13879–89. Available: <https://doi.org/10.1021/acsami.6b01850>.
31. Chen J, Zhao D, Diao Z, Wang M, Shen S. Ferrites boosting photocatalytic hydrogen evolution over graphitic carbon nitride: A case study of (Co, Ni) $Fe_2O_4$  modification. *Science Bulletin* 2016; 61:292–301. Available: <https://doi.org/10.1007/s11434-016-0995-0>.
32. Obregón S, Colón G. Improved  $H_2$  production of Pt- $TiO_2/g-C_3N_4-MnO_x$  composites by an efficient handling of photogenerated charge pairs. *Applied Catalysis B: Environmental* 2014;144:775–82. Available: <https://doi.org/10.1016/j.apcatb.2013.07.034>.
33. Fu J, Chang B, Tian Y, Xi F, Dong X. Novel  $C_3N_4-CdS$  composite photocatalysts with organic-inorganic heterojunctions: In situ synthesis, exceptional activity, high stability and photocatalytic mechanism. *Journal of Materials Chemistry A* 2013;1: 3083–90. Available: <https://doi.org/10.1039/c2ta00672c>.
34. Huang L, Xu H, Li Y, Li H, Cheng X, Xia J, et al. Visible-light-induced  $WO_3/g-C_3N_4$  composites with enhanced photocatalytic activity. *Dalton Transactions* 2013;42: 8606–16. Available: <https://doi.org/10.1039/c3dt00115f>.

### SUPPORTING INFORMATION

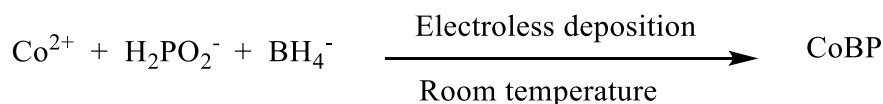


Fig. S1. Schematic illustration of the formation of amorphous CoBP sample

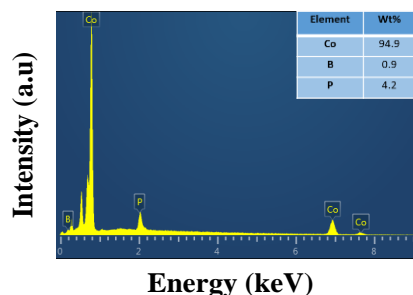


Fig. S2. High resolution XPS spectra of (a) Co 2p region. (b) P 2p region. (c) B 1s region for CoBP sample

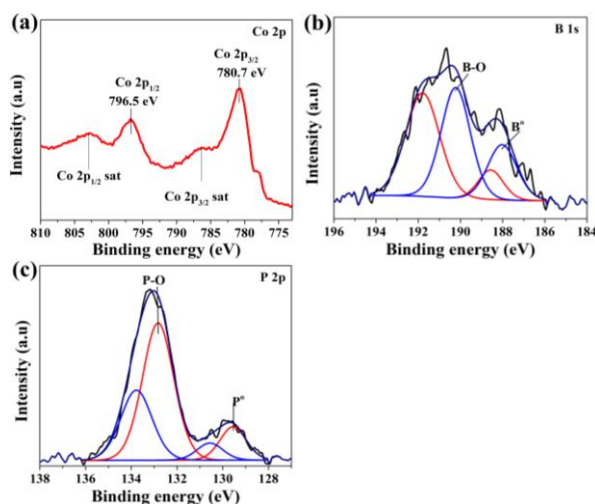


Fig. S3. High resolution XPS spectra of (a) Co 2p region. (b) P 2p region. (c) B 1s region for CoBP sample

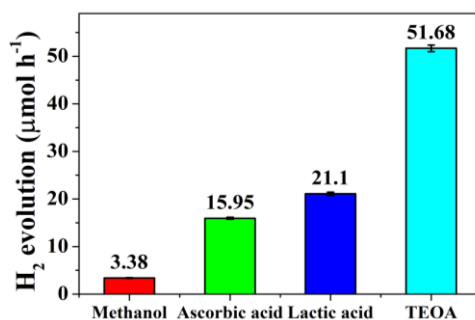


Fig. S4. Comparison of photocatalytic hydrogen evolution rates on C<sub>3</sub>N<sub>4</sub>/5 wt% CoBP composite photocatalyst in the presence of different sacrificial reagents under visible light ( $\lambda \geq 420$  nm). Reaction conditions: Catalyst, 50 mg; 100 mL of solution containing sacrificial reagents; light source, xenon lamp (300 W) with a cutoff filter; temperature, 10 °C



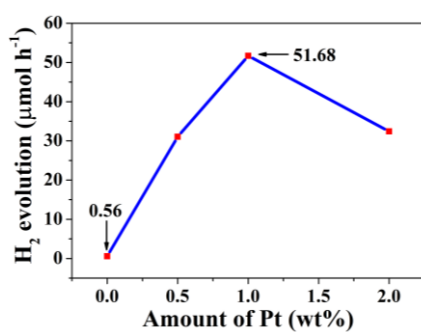


Fig. S5. Effect of the Pt loading amounts on photocatalytic hydrogen evolution of C<sub>3</sub>N<sub>4</sub>/5 wt% CoBP under visible light irradiation ( $\lambda \geq 420$  nm)

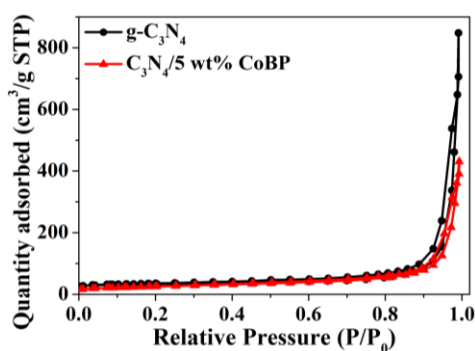


Fig. S6. Nitrogen adsorption-desorption isotherms of pure g-C<sub>3</sub>N<sub>4</sub> and C<sub>3</sub>N<sub>4</sub>/5 wt% CoBP composite photocatalysts

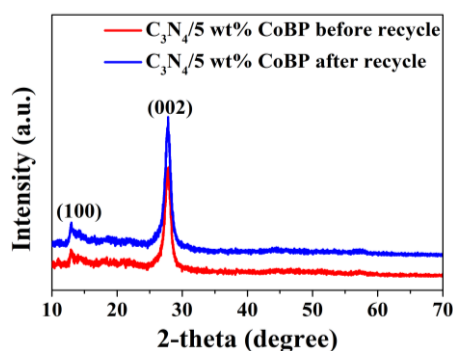


Fig. S7. XRD spectra of C<sub>3</sub>N<sub>4</sub>/5 wt% CoBP composite photocatalysts before and after recycle

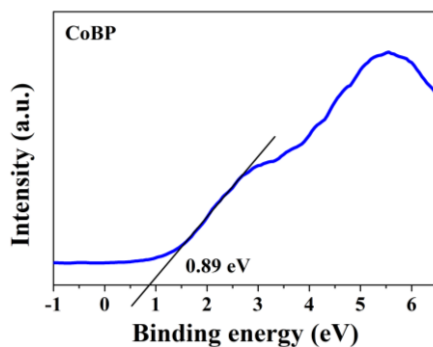


Fig. S8. Valence band XPS spectra of CoBP sample

**Table S1. Fitting parameters of EIS results**

Samples	Rs	Rct
g-C <sub>3</sub> N <sub>4</sub> photocatalysts	25.67	686.1
C <sub>3</sub> N <sub>4</sub> /5 wt% CoBP composite photocatalysts	19.58	652.1

**Table S2. Comparison of the hydrogen production activity and AQY value of various g-C<sub>3</sub>N<sub>4</sub>-based heterostructure photocatalysts reported previously**

Photocatalysts	Pt [wt%]	Light source	HER $\mu\text{molh}^{-1}\text{g}^{-1}$	AQY [%]	Refs.
g-C <sub>3</sub> N <sub>4</sub> /CoTPP	1	300 W Xe lamp ( $\lambda \geq 420$ nm)	938.6	4.2 ( $\lambda = 420$ nm)	[6]
CoTiO <sub>3</sub> /g-C <sub>3</sub> N <sub>4</sub>	3	300 W Xe lamp (under simulated solar light irradiation)	858	3.23 ( $\lambda = 420$ nm)	[30]
g-C <sub>3</sub> N <sub>4</sub> /CoFe <sub>2</sub> O <sub>4</sub>	1	300 W Xe lamp ( $\lambda > 420$ nm)	186.1	3.35 ( $\lambda = 420$ nm)	[31]
g-C <sub>3</sub> N <sub>4</sub> /CoO	3	300 W Xe lamp ( $\lambda \geq 400$ nm)	651.3	NA	[16]
C <sub>3</sub> N <sub>4</sub> /CoBP	1	300 W Xe lamp ( $\lambda \geq 420$ nm)	1033.6	5.42 ( $\lambda = 420$ nm)	Our work

© Copyright (2024): Author(s). The licensee is the journal publisher. This is an Open Access article distributed under the terms of the Creative Commons Attribution License (<http://creativecommons.org/licenses/by/4.0>), which permits unrestricted use, distribution, and reproduction in any medium, provided the original work is properly cited.

Peer-review history:  
The peer review history for this paper can be accessed here:  
<https://www.sdiarticle5.com/review-history/115156>